ISSN 0036-0236, Russian Journal of Inorganic Chemistry, 2024. © Pleiades Publishing, Ltd., 2024.

PHYSICAL CHEMISTRY OF SOLUTIONS

Spin Crossover in Dimethyl Sulfoxide Solutions of an Iron(II) Perrhenate Complex with 2,6-Bis(Benzimidazol-2-yl)Pyridine

V. V. Kokovkin[a], *, I. V. Mironov[a], E. V. Korotaev[a], and L. G. Lavrenova[a]

[a] *Nikolaev Institute of Inorganic Chemistry, Siberian Branch, Russian Academy of Sciences, Novosibirsk, 630090 Russia*

**e-mail: basil@niic.nsc.ru*

Received September 8, 2023; revised November 23, 2023; accepted November 24, 2023

Abstract—Dimethyl sulfoxide (DMSO) solutions of $[FeL_2](ReO_4)_2 \cdot 1.5H_2O$ (**1**), the iron(II) perrhenate complex with 2,6-bis(benzimidazol-2-yl)pyridine (L), are characterized by physicochemical methods, namely, by static magnetic susceptibility measurements, conductometry, and UV–Vis spectrophotometry. As found previously, complex **1** exhibits a sharp high-temperature spin crossover (SCO): $^1A_1 \leftrightarrow {}^5T_2$. The temperature-dependent $\mu_{eff}(T)$ study of complex **1** in DMSO showed that the SCO also manifests itself in solution. The 298 K electrical conductivity of DMSO solutions implies that complex **1** is almost completely dissociated in the range of concentrations studied from 3.6×10^{-6} to 9.12×10^{-4} mol/L. An absorption peak is found in the UV region of the spectrum, which is almost independent of temperature. In the visible region, two combined absorption peaks are observed at 520–560 nm, responsible for FeL^{2+} and FeL_2^{2+} complex formation and varying with temperature and L concentration.

Keywords: complex formation, iron(II), 2,6-bis(benzimidazol-2-yl)pyridine, spectrophotometry, conductivity measurements, spin-crossover

DOI: 10.1134/S0036023623603197

INTRODUCTION

Spin crossover (SCO) [1, 2] is a phenomenon that invariably attracts attention and has been the subject matter of numerous studies [3–16]. A reversible change in the spin multiplicity of the central atom (low spin (LS) ↔ high spin (HS)) can be observed in transition-metal complexes with the $3d^4$–$3d^7$ electronic configuration, having an octahedral or pseudo-octahedral geometry of the coordination polyhedron. Spin crossover manifests itself under the influence of external conditions: temperature, pressure, exposure to the light of a certain wavelength, external electric or magnetic field, and other factors. Compounds that exist in two spin states each with a sufficiently long lifetime can be used to develop molecular electronics devices, in particular for creating displays, memory systems, and in other areas. The brightest manifestations of SCO are in iron(II) complexes with polynitro heterocyclic ligands. These compounds are of particular interest due to the thermochromism accompanying SCO: $^1A_1$ (S = 0, LS) ↔ $^5T_2$ (S = 2; HS) in them. This significantly expands the application range of these complexes, for example, in MRI as contrast agents [6]. Recently, much attention has been paid to the search for compounds exhibiting bifunctional properties. [17–22].

Complexes exhibiting SCO in the solid state are studied by static magnetic susceptibility, Mössbauer spectroscopy, and by other methods. Sufficient attention is also paid to the characterization of complexes that exhibit SCO in solutions [23–28]. Toftlund [28] made a great contribution to the progress in relevant research. The nature of SCO in the solid phase of complexes depends on many factors, including sample preparation. A simpler situation can be expected in solutions, for there are no "lattice effects" as in the solid state.

The Novosibirsk research team has been engaged for a number of years in the design, synthesis, and characterization of iron(II) complexes with a number of polynitro heterocycles, in particular with derivatives of 1,2,4-triazole [29], tris(pyrazol-1-yl)methane [11], and 2,6-bis(1*H*-imidazol-2-yl)pyridine [12]. Most of these compounds exhibit sharp SCO with a hysteresis on $\mu_{eff}(T)$ curves. The results of studying solutions of iron(II) complexes with 4-amino-1,2,4-triazole and tris(pyrazol-1-yl)methane were published previously [30, 31].

The goal of this work was to study the SCO in an iron(II) perrhenate complex with 2,6-bis(benzimidazol-2-yl)pyridine (L) in dimethyl sulfoxide (DMSO) solution. The investigation tools used were static magnetic susceptibility measurements, conductometry,

and UV–Vis spectrophotometry. The solid complex $[FeL_2](ReO_4)_2 \cdot 1.5H_2O$ has a sharp SCO with a hysteresis [32].

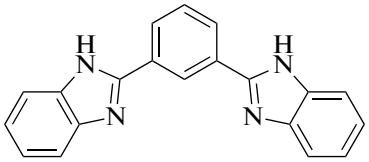

Scheme 1. 2,6-Bis(benzimidazol-2-yl)pyridine (L).

EXPERIMENTAL

The chemicals used in the work were $FeSO_4 \cdot 7H_2O$ (Acros Organics), $NaReO_4$ (Alfa Aesar), ascorbic acid ("med." grade), 2,6-bis(imidazol-2-yl)pyridine (L, Sigma-Aldrich), and DMSO (specialty grade). All chemicals were used as received.

The $[FeL_2](ReO_4)_2 \cdot 1.5H_2O$ (**1**) was prepared as described elsewhere [32]. The characterization showed that compound **1** has a distorted octahedral geometry of the coordination polyhedron. Two 2,6-bis(benzimidazol-2-yl)pyridine molecules are coordinated to an iron(II) ion in the tridentate-cyclic mode via two nitrogen atoms of imidazole rings and the pyridine nitrogen atom to form the FeN_6 coordination core. For testing the methodology and comparing the results, the salt $Fe(ReO_4)_2$ (**2**) was first prepared, by dissolving a weight of $FeSO_4 \cdot 7H_2O$ in water acidified with ascorbic acid, adding a one-and-a-half excess of $NaReO_4$, and then partially concentrating the resulting solution by incomplete evaporation. The $Fe(ReO_4)_2$ precipitated in about one day after the components were mixed.

The solvent used was DMSO, which was preliminary purged with argon to remove trace oxygen in order to prevent iron(II) oxidation.

The static magnetic susceptibility of samples was measured by the Faraday method in the range 80–420 K. Temperature stabilization of the sample with an accuracy of 1 K during measurement was carried out using a DTB9696 (DeltaElectronics) PID controller. The heating and cooling rates were ca. 2–3 K/min. The external magnetic field strength of 7.3 kOe was maintained during the studies with a stabilization accuracy of ca. 1%. When the dehydrated complex was studied, the sample was placed in an open quartz ampoule, and the measurement cell of the setup was evacuated to a residual pressure of 10^{-2} mmHg; then an inert helium atmosphere was created at a pressure of 5 mm Hg. When the intact complex or its 0.0025 M solution in DMSO was studied, the test samples were sealed with atmospheric air in quartz ampoules. The magnetic susceptibility of the complex in solution was calculated as the difference between the magnetic susceptibilities of the solution and DMSO. The effective magnetic moment was calculated as $\mu_{eff} = (8\chi'_M T)^{1/2}$, where χ'_M is the molar magnetic susceptibility corrected for the diamagnetic contribution using Pascal's scheme. The temperatures of the direct ($T_c\uparrow$) and reverse ($T_c\downarrow$) transitions in the complex were determined based on the condition $d^2\mu_{eff}/dT^2 = 0$.

The DMSO solutions of the $[Fe(L)_2](ReO_4)_2 \cdot 1.5H_2O$ and $Fe(ReO_4)_2$ test compounds were prepared in a box filled with argon. The DMSO was also purged with argon before it was used to prepare solutions in order to remove oxygen. The solutions were prepared by dissolving weights of compounds **1** and **2** in the set volumes of the solvent.

The electrical conductivity of solutions was measured on a Radelkis OK-102/1 conduction meter. The measurements were carried out at concentrations in the range from 1.23×10^{-5} to 9.12×10^{-4} mol/L for complex **1** and 7.97×10^{-6} to 0.0020 mol/L for $Fe(ReO_4)_2$. The upper concentration bounds roughly correspond to the solubilities of the test compounds in DMSO. Electrical conductivity values were converted to specific electrical conductivities (æ) using a cell constant, which was determined from measurements in KCl aqueous solutions of known concentration (æ = 0.001413 S/cm for 0.0100 mol/L at 25°C).

Absorption spectra were measured on a Genesis-6 spectrophotometer in tightly closed cells with $l = 0.10$, 0.5, and 1 cm in the wavelength range 300–800 nm. A temperature-controlled unit connected to an external water thermostat was used to change the cell temperature.

RESULTS AND DISCUSSION

Static Magnetic Susceptibility

Figure 1 illustrates the results of magnetic susceptibility measurements of intact complex **1**, its dehydrated analogue, and its DMSO solution. Complex **1** exhibits SCO both in the intact and dehydrated (**1a**) solid states and in the DMSO solution (**1s**). The direct and reverse transition temperatures are listed in Table 1. The first thing to be mentioned here is the change in effective magnetic moment and the maintenance of the hysteresis between the direct and reverse transitions after complex **1** is dissolved in DMSO. In the high-spin state, complex **1s** exhibits a higher reachable value of μ_{eff} (4.88 μ_B) than the intact (**1**, 4.27 μ_B) or dehydrated (**1a**, 4.51 μ_B) complex does. The respective value is in a better agreement with the theoretical value (4.9 μ_B) for the Fe^{2+} ion [33–35] than the values for intact complex **1** and its dehydrated analogue **1a** are. This fact may indicate that in a solid sample in a high-spin state, some of the iron ions retain their low-spin state, while in solutions their fraction is significantly smaller. In the low-spin state, complex **1s** is diamagnetic, and it exhibits no residual magnetic moment, which is observed for **1** (0.49 μ_B) and **1a** (0.73 μ_B). The occurrence of a residual magnetic moment in com-

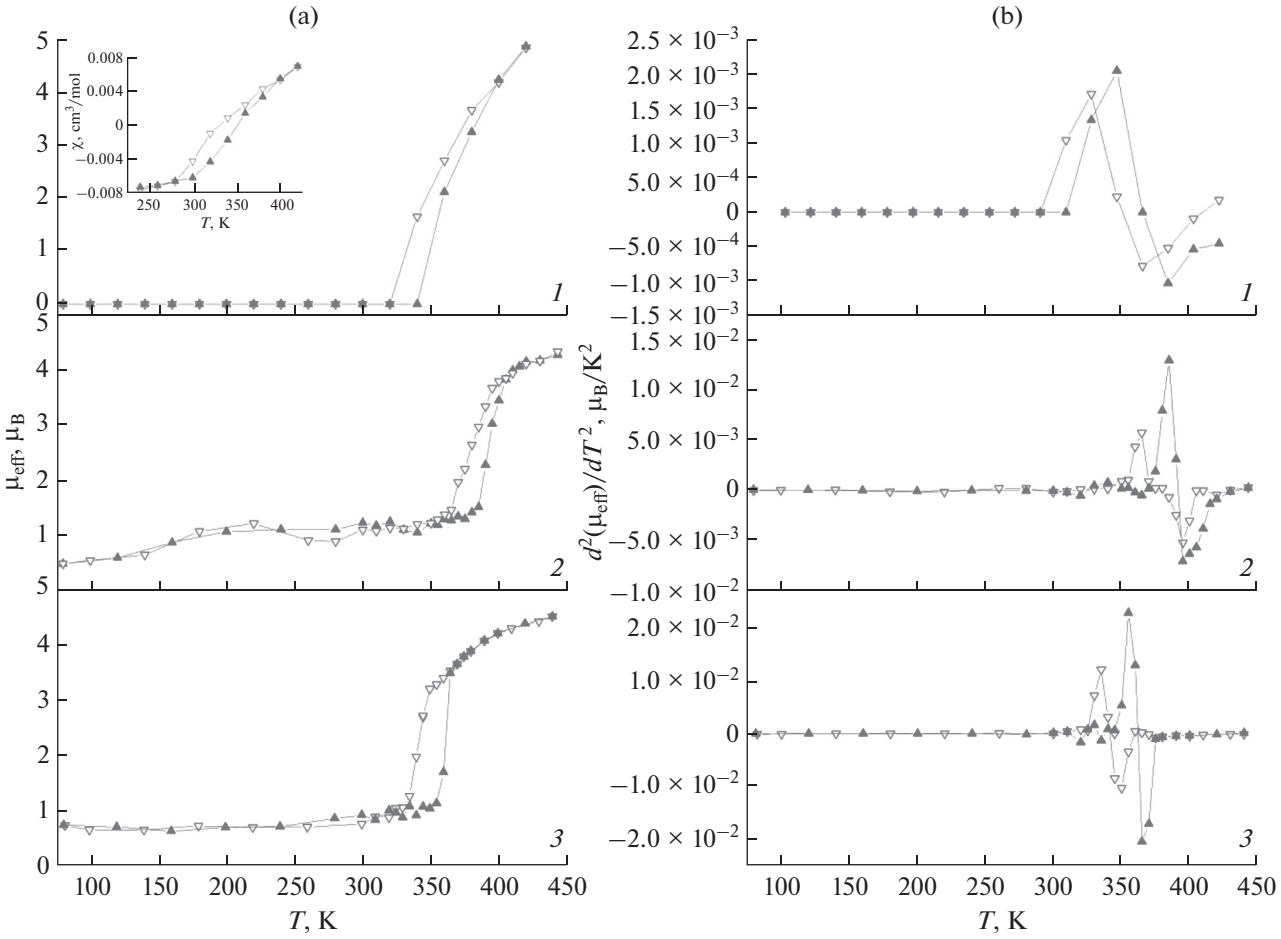

Fig. 1. Temperature-dependent (a) μ_{eff} and (b) $d(\mu_{eff})^2/dT^2$ plots for (*1*) complex **1s**, (*2*) complex **1**, and (*3*) complex **1a** (▲ heating; ▽ cooling). In the inset, the temperature-dependent magnetic susceptibility is plotted for temperature-dependent μ_{eff} in the case of complex **1s**.

plexes **1** and **1a** may be due to their temperature-independent Van Vleck paramagnetism. Thus, we may conclude that a more complete transition is observed for complex **1s** than for samples **1** and **1a**. In terms of the temperatures of forward and back transitions, the highest values correspond to intact complex **1**. The dehydration of the intact complex and its dissolution in DMSO decrease the crossover temperature; the temperature ranges in which spin crossover occurs for complexes **1a** and **1s** overlap. Complex **1s** shows the lowest direct transition temperature, while the reverse transition temperature in **1a** is lower. Noteworthy is also a significant hysteresis between the direct and reverse transitions, observed for all the studied compounds both directly in the temperature-dependent μ_{eff} and in its second derivative (Fig. 1). The dehydration of complex **1** and its dissolution in DMSO are accompanied with an increase in hysteresis between the direct and reverse transitions. The greatest hysteresis corresponds to complex **1a**, while complex **1s** exhibits an intermediate value of hysteresis between the ΔTs for **1** and **1a**.

Thus, our studies show that complex **1** also exhibits spin crossover when dissolved in DMSO. Not only does dissolution changes its effective magnetic moment, but it also affects the spin-crossover temperature and the hysteresis magnitude.

Conductivity Measurements

This study was arranged to provide a primary characterization of the system. Figure 2 shows the logæ versus log$C$ plots for DMSO solutions of complex **1** and complex **2** with various concentrations. The plots

Table 1. Direct ($T_c\uparrow$) and reverse ($T_c\downarrow$) transition temperatures for the compounds studied

Compound	$T_c\uparrow$, K	$T_c\downarrow$, K	ΔT_c, K
1s	360	345	15
1	392	381	11
1a	362	341	21

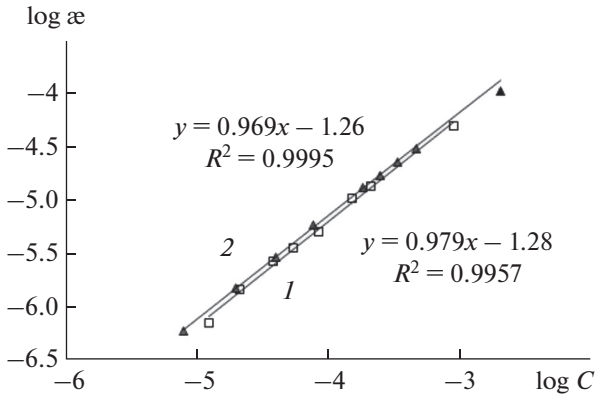

Fig. 2. Electrical conductivity (æ) versus concentration for DMSO solutions at $T = 25°C$: (*1*) $[FeL_2](ReO_4)_2 \cdot 1.5H_2O$ and (*2*) $Fe(ReO_4)_2$.

each have a slight curvature with a mid-section slope of about 0.979 for **1** and 0.969 for **2**.

The conductometric data for **1** can help to estimate the average equivalent electrical conductivity of the electrolyte in DMSO, which is $\Lambda^0_{DMSO}(\mathbf{1}) = 1000 \times æ/C = 32.3$ (S cm^2)/equiv. Referring to an aqueous solution was carried out using the Walden–Pisarzhevsky rule [36]:

$$\Lambda^0_{H_2O} = \Lambda^0_{DMSO} \frac{\eta_{DMSO}}{\eta_{H_2O}}, \quad (1)$$

where Λ^0 is the maximum equivalent electrical conductivity of complex **1** in water and in DMSO, and η is the dynamic viscosity of the solvent.

The dynamic viscosities η for DMSO and water at 25°C are 1.967×10^{-3} and 0.896×10^{-3} Pa s, respectively. Referring to an aqueous solution using Eq. (1) yields $\Lambda^0_{H_2O} = 71.0$ (S cm^2)/equiv. For $Fe(ReO_4)_2$, the average value in the range of concentrations studied is $\Lambda^0_{DMSO} = 36.3$ (S cm^2)/equiv. The value obtained when referred to an aqueous solution by Eq. (1), $\Lambda^0_{H_2O} = 80.0$ (S cm^2)/equiv, is far lower than the value calculated with the $\lambda^0_{H_2O}$ known for Fe^{2+} and ReO_4^- [37] on the assumption of complete dissociation: $\lambda^0_{H_2O}(1/2Fe^{2+}) + \lambda^0_{H_2O}(ReO_4^-) = 108.4$ (S cm^2)/equiv. Therefore, in view of the near-unity slope of the log æ versus log C plot (Fig. 2), we may conclude that $Fe(ReO_4)_2$ in DMSO is completely dissociated only at the first step.

Referring the aqueous solution data for ReO_4^- to DMSO solution gives $\lambda^0_{DMSO}(ReO_4^-) = 25.0$ (S cm^2)/equiv. Since the total value Λ^0_{DMSO} (1) = 32.3 (S cm^2)/equiv, the share of the large complex cation $[FeL_2]^{2+}$, which has a chelate structure, accounts for $\lambda^0_{DMSO}(1/2Fe^{2+}) = 7.3$ (S cm^2)/equiv. Thus, complex **1** exists in DMSO solutions without outer-sphere ReO_4^- ions. Evidence for this also comes from the linearity of log æ versus log C dependence, which should have a slope of 1.0 because of the electrical conductivity of DMSO. Figure 2 supports this, too. It should be mentioned that the conductivity measurements were carried out at 25°C for a short time (within 20–30 min). This is unlikely because of the general slowness of transformations that FeL_2^{2+} would have largely converted to FeL^{2+}, although this transformation would not have greatly affected the results since L has the zero charge.

Spectrophotometric Measurements

The magnetic moment hysteresis (Fig. 1a), i.e., the discrepancy between the temperature dependences measured during heating and cooling for complexes in solution, can only be caused by a lack of equilibrium between the species due to their slow transformation into one another. In this case, the concentrations of the species at the same temperature will not coincide upon heating and cooling. Two species may be expected to exist at $C_L/C_{Fe} \geq 2$ in the system under consideration, namely, FeL^{2+} and FeL_2^{2+}, the more so as the stability of chelate complexes always decreases significantly as temperature rises [38]. DMSO molecules also can be ligands, but we do not mention them as their concentration is high and constant. Conductometry data imply that ReO_4^- ions are almost not associated with FeL_2^{2+}. There is only one work where $FeL^{2+} + L = FeL_2^{2+}$ equilibrium was studied [23]. However, methanol was chosen as a solvent, which does not allow us to use these results here. As mentioned above, the complexation rates in the selected solvent are low and equilibrium is not achieved, at least at low temperatures. The magnetic measurements imply that FeL_2^{2+} LS species and FeL_2^{2+} HS species simultaneously occur in the solution over a wide range of temperatures (Fig. 1), while usually these species have different stabilities. It is, however, difficult to say exactly which of the subsystems (LS or HS) is more inert.

When transformations are slow, the absorption spectra, too, can feature a discrepancy between the records made upon heating and cooling (a hysteresis), qualitatively like in magnetic moments. The bands due to *d–d* transitions are usually paid much attention in crossover studies. In the system under consideration, however, these bands are completely overlapped by the far stronger charge-transfer bands. The spectrum shown in Fig. 3 refers to both of the FeL^{2+} and FeL_2^{2+} species. It changes significantly in response to changing temperature. In the exemplary spectrum shown in

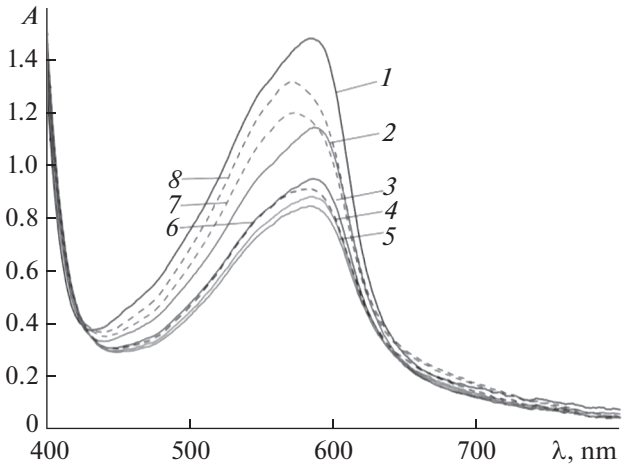

Fig. 3. Spectrum of the DMSO solution containing $[FeL_2](ReO_4)$ (3.6×10^{-4} mol/L) and L (1.83×10^{-3} mol/L); $l = 1$ cm. Solid lines are heating curves: (*1*) 25, (*2*) 35, (*3*) 45, (*4*) 55, and (*5*) 65°C; dashed lines show cooling curves: (*6*) 55, (*7*) 40, and (*8*) 25°C.

Fig. 3, the peak intensity is reduced about twofold upon heating to 65°C (at ca. 1 K/min). The peak position changes only insignificantly (<2 nm). Cooling back to the initial temperatures, however, brings about both a noticeable evolution of the spectrum and a shift of the peak from 586 to 572 nm. The peak intensity is reduced by 16% compared to that before heating. A similar picture is observed in other cases: the spectrum after cooling never coincides with the initial one (recorded before heating), and it has lower peak intensity.

This trend correlates with the magnetic susceptibility hysteresis (the inset for **1s** in Fig. 1a) in the range of room temperatures. The LS state of iron ions prevails in this temperature range; the magnetic susceptibility is negative ($\mu_{eff} = 0$) and continues to decrease. The curves corresponding to heating and cooling of the sample begin to coincide in the temperature range less than 280 K.

In addition to the band shown in Fig. 3, the spectrum of the complex features a strong band at 330 nm with $\varepsilon = 1.8 \times 10^4$, whose characteristics are completely independent of temperature. Apparently, this is an intraligand band due to $\pi-\pi$ transitions in L.

The ReO_4^- ion does not absorb in the used spectral range. A strong absorption of DMSO is observed at $\lambda < 300$ nm.

CONCLUSIONS

The iron(II) perrhenate complex with 2,6-bis(benzimidazol-2-yl)pyridine (L) of composition $[FeL_2](ReO_4)_2 \cdot 1.5H_2O$ in DMSO has been characterized by physicochemical methods, namely, by static magnetic susceptibility measurements, conductometry, and UV–Vis spectrophotometry. The complex exhibits sharp spin crossover both in solid (intact and dehydrated) state and in DMSO solutions. The direct and reverse spin transition temperatures have been determined.

The spectra of solutions in the region of charge-transfer bands also strongly depend on temperature: the bands have their intensities decreasing upon heating and increasing upon cooling, but the spectra are not completely restored after cooling to the initial temperature. The observed discrepancies (hysteresis) are explained by the processes slowed down upon complex formation.

FUNDING

This work was supported by the Ministry of Science and Higher Education of the Russian Federation (project Nos. 121031700315-2 and 121031700313-8).

CONFLICT OF INTEREST

The authors declare that they have no conflicts of interest.

REFERENCES

1. P. Gütlich and H. Goodwin, in *Topics in Current Chemistry*, vols. **233–235** (Springer, Berlin, 2004).
2. M. A. Halcrow, *Spin-Crossover Materials Properties and Applications* (J. Wiley & Sons Ltd., U.K., 2013).
3. K. S. Kumar and M. Ruben, Coord. Chem. Rev. **346**, 176 (2017). https://doi.org/10.1016/j.ccr.2017.03.024
4. H. S. Scott, R. W. Staniland, and P. E. Kruger, Coord. Chem. Rev. **362**, 24 (2018). https://doi.org/10.1016/j.ccr.2018.02.001
5. X. Yang, A. Enriquez-Cabrera, D. Dorian Toha, et al., Dalton Trans. **52**, 10828 (2023). https://doi.org/10.1039/d3dt02003g
6. O. Kahn, J. Krober, and C. Jay, Adv. Mater. **4**, 718 (1992). https://doi.org/10.1002/adma.19920041103
7. A. Enriquez-Cabrera, A. Rapakousiou, M. P. Bello, et al., Coord. Chem. Rev. **419**, 213396 (2020). https://doi.org/10.1016/j.ccr.2020.213396
8. K. S. Kumar, S. Vela, B. Heinrich, et al., Dalton Trans. **49**, 1022 (2020). https://doi.org/10.1039/C9DT04411F
9. S. K. Kuppusamy, A. Mizuno, A. Garcia-Fuente, et al., ACS Omega **7**, 13654 (2022). https://doi.org/10.1021/acsomega.1c07217
10. G. Molnar, S. Rat, L. Salmon, et al., Adv. Mater. **30**, 1703862 (2018). https://doi.org/10.1002/adma.201703862
11. O. G. Shakirova and L. G. Lavrenova, Crystals **10**, 843 (2020). https://doi.org/10.3390/cryst10090843
12. L. G. Lavrenova and O. G. Shakirova, Russ. J. Inorg. Chem. **68**, 690 (2023). https://doi.org/10.1134/S0036023623600764

13. W. Guo, N. Daro, S. Pillet, et al., Chem.-Eur. J. **26**, 12927 (2020). https://doi.org/10.1002/chem.202001821
14. P. O. Ribeiro, B. P. Alho, R. M. Ribas, et al., J. Magn. Magn. Mater. **489**, 165340 (2019). https://doi.org/10.1016/j.jmmm.2019.165340
15. E. Cuza, C. D. Mekuimemba, N. Cosquer, et al., Inorg. Chem. **60**, 6536 (2021). https://doi.org/10.1021/acs.inorgchem.1c00335
16. A. R. Craze, H. Zenno, M. C. Pfrunder, et al., Inorg. Chem. **60**, 6731 (2021). https://doi.org/10.1021/acs.inorgchem.1c00553
17. M. Piedrahita-Bello, J. E. Angulo-Cervera, R. Courson, et al., J. Mater. Chem. **8**, 6001. https://doi.org/10.1039/D0TC01532F
18. T. D. Nguyen, J. M. Veauthier, G. F. Angles-Tamayo, et al., J. Am. Chem. Soc. **142**, 4842 (2020). https://doi.org/10.1021/jacs.9b13835
19. B.-X. Luo, Y. Pan, Y.-Sh. Meng, et al., Eur. J. Inorg. Chem. **38**, 3992 (2021). https://doi.org/10.1002/ejic.202100622
20. R. Turo-Cortes, M. Meneses-Sanchez, T. Delgado, et al., J. Mater. Chem. C **10**, 10686 (2022). https://doi.org/10.1039/D2TC02039D
21. N. M. J. N. Ibrahim, S. M. Said, A. Mainal, et al., Mater. Res. Bull. **126**, 110828 (2020). https://doi.org/10.1016/j.materresbull.2020.110828
22. P. J. Ribeiro, B. P. Alho, R. M. Ribas, et al., J. Magn. Magn. Mater. **489**, 165340 (2019). https://doi.org/10.1016/j.jmmm.2019.165340
23. B. Strauss, W. Linert, V. Gutmann, et al., Monatsh. Chem. **123**, 537 (1992).
24. M. Boca, R. F. Jameson, and W. Linert, Coord. Chem. Rev. **255**, 290 (2011). https://doi.org/10.1016/j.ccr.2010.09.010
25. I. Bräunlich, A. Sánchez-Ferrer, M. Bauer, et al., Inorg. Chem. **53**, 3546 (2014). https://doi.org/10.1021/ic403035u
26. S. Sundaresan, J. A. Kitchen, and S. Brooker, Inorg. Chem. Front. **7**, 2050 (2020). https://doi.org/10.1039/c9qi01478k
27. I. Nikovskiy, A. Polezhaev, V. Novikov, et al., Chem.-Eur. J. **26**, 5629 (2020). https://doi.org/10.1002/chem.202000047
28. H. Toftlund, Coord. Chem. Rev. **94**, 67 (1989).
29. L. G. Lavrenova and O. G. Shakirova, Eur. J. Inorg. Chem, **5–6**, 670 (2013). https://doi.org/10.1002/ejic.201200980
30. V. V. Kokovkin, I. V. Mironov, E. V. Korotaev, et al., Chem. Select **4**, 9360 (2019). https://doi.org/10.1002/slct.201901424
31. V. V. Kokovkin, E. V. Korotaev, I. V. Mironov, et al., J. Struct. Chem. **62**, 1191 (2021). https://doi.org/10.1134/S0022476621080047
32. L. G. Lavrenova, I. I. Dyukova, E. V. Korotaev, et al., Russ. J. Inorg. Chem. **65**, 30 (2020). https://doi.org/10.1134/S0036023620010106
33. P. W. Selwood, *Magnetochemistry* (Pierce Wilson, 1956).
34. Yu. V. Rakitin and V. T. Kalinikov, *Modern Magnetochemistry* (Nauka, St. Petersburg, 1994) [in Russian].
35. K. Day and D. Selbin, *Theoretical Inorganic Chemistry* (Khimiya, Moscow, 1976) [in Russian].
36. B. B. Damaskin, O. A. Petriy, and G. A. Tsirlina, *Electrochemistry* (Lan', Moscow, 2015) [in Russian].
37. D. Dobos, *Electrochemical Data: A Handbook for Electrochemists* (Elsevier, New York, 1975).
38. M. G. Nikitina and D. F. Pyreu, Russ. J. Inorg. Chem. **66**, 1569 (2021). https://doi.org/10.1134/S0036023621100120

Translated by O. Fedorova